JPhys Materials

PAPER • OPEN ACCESS

Bimodal polarons as a function of morphology in high efficiency polymer/acceptor blends for organic photovoltaics

To cite this article: Junjun Guo *et al* 2021 *J. Phys. Mater.* **4** 044009

Journal of Physics: Materials

OPEN ACCESS

RECEIVED
17 March 2021

REVISED
2 June 2021

ACCEPTED FOR PUBLICATION
29 June 2021

PUBLISHED
14 July 2021

PAPER

Bimodal polarons as a function of morphology in high efficiency polymer/acceptor blends for organic photovoltaics

Junjun Guo, Jose M Marin-Beloqui and Tracey M Clarke*

Department of Chemistry, University College London, Christopher Ingold Building, London WC1H 0AJ, United Kingdom
* Author to whom any correspondence should be addressed.

E-mail: tracey.clarke@ucl.ac.uk

Keywords: conjugated polymer, organic photovoltaics, solar cell, polaron, triplet, transient absorption spectroscopy, photophysics

Supplementary material for this article is available online

Abstract

The polymer PffBT4T-C9C13 (poly[(5,6-difluoro-2,1,3-benzothiadiazole-4,7-diyl)[3,3‴-bis (2-decyltetradecyl)[2,2′:5′,2″:5″,2‴ -quaterthiophene]-5,5‴-diyl]]) produces organic solar cells of >11% efficiency with both fullerenes and non-fullerenes. We present a comprehensive morphology and spectroscopy study of this polymer and its blends, focusing on atomic force microscopy, x-ray diffraction, and transient absorption spectroscopy on microsecond timescales. Unusually, fullerene-induced ordering is observed, with the polymer/fullerene blend displaying a greater crystallinity compared to the pristine polymer. This was correlated with the appearance of bimodal polarons: fast-decaying polarons in the pristine amorphous polymer domains and trapped polarons localised in the fullerene-induced ordering (crystallline) domains. The lifetime of the trapped polaron was significantly enhanced upon thermal annealing, and the complex relationship observed between lifetime and film crystallinity suggest a contribution from trap states at the interfaces between ordered and disordered domains that lead to inhibited recombination. In contrast, blends incorporating the well-known analogue PffBT4T-2OD (with a shorter alkyl chain length) exhibit neither fullerene-induced ordering nor bimodal polarons. However, both PffBT4T-C9C13 and PffBT4T-2OD polymer blends show clear evidence of polymer triplet formation, which is the first time triplets have been identified in PffBT4T-based blends. In this study, we remark upon the complex relationship between morphology and the photophysics. This relationship will open the door to the synthesis of new molecules to control the blend morphology and thus optimise organic photovoltaic performance.

1. Introduction

Organic photovoltaics (OPV) have attracted considerable attention in recent years due to their flexibility, versatility, and solution processability. These factors enable industrial manufacture scale and reduce the energy payback time to as short as a single day [1]. Bulk heterojunction solar cells based on an interpenetrating network of an electron donor and fullerene electron acceptor have shown power conversion efficiencies for single junction devices of >18% [2]. In organic solar cells, this donor/acceptor interpenetrating network is necessary to achieve efficient exciton dissociation. However, a donor/acceptor blend that is too intermixed results in high levels of charge recombination and inhibits the charge carriers from reaching the electrodes. As such, it is vitally important to control the morphology of the blend films to achieve an optimal device efficiency [3].

The conjugated polymer poly[(5,6-difluoro-2,1,3-benzothiadiazol-4,7-diyl)-alt-(3,3‴-di (2-nonyltridecyl)-2,2′;5′,2″;5″,2′ ″ -quaterthiophen-5,5‴-diyl)] (PffBT4T-C9C13) is capable of device efficiencies of over 11% [4]. A series of PffBT4T polymers exist, with a range of alkyl chain lengths. These polymers, such as PffBT4T-2OD and PffBT4T-2DT, show strong interchain aggregation in solution at room temperature [5]. Heating polymer solutions above 60 °C causes the aggregation to disperse. The

temperature-dependent aggregation of these polymers is independent of the choice of acceptor. A key element of this behaviour is that it can be utilized to create the near-ideal polymer/acceptor morphology, containing highly crystalline polymer domains, by controlling the temperature and time for polymer aggregation [6]. In addition to tuning morphology using solution temperature, further modifications to the polymer blend morphology can be achieved using processing additives and thermal annealing [6]. Due to their temperature-dependent aggregation properties, PffBT4T-based polymers have attracted a great deal of attention for morphology studies. However, spectroscopy and photophysical studies for these high-efficiency polymers are scarce [7, 8], especially for PffBT4T-C9C13. Of particular interest, however, is how the fine-tuning of morphology enabled by these polymers affects their photophysical properties. We will focus on fullerene blends, primarily because fullerenes' transient species are well-characterised and of weak absorption cross-section, thereby enabling the polymer transient species to dominate the spectra.

In this paper, microsecond transient absorption spectroscopy (TAS) is employed to directly monitor charge photogeneration and recombination in PffBT4T-C9C13:$PC_{70}BM$ and PffBT4T-2OD:$PC_{70}BM$ films as a function of different morphology tuning methodologies. Microsecond TAS is an ideal technique for this purpose, as the polaron yield observed is directly proportional to both device short circuit current and external quantum efficiency [9, 10]. Furthermore, it allows for the influence of other species—such as triplets—to be identified. Finally, and crucially for our purpose here, TAS can resolve different polaron types: bulk versus interfacial polarons have been observed [11], and also delocalised versus localised polarons [12]. Furthermore, the morphologies of each film are characterised using atomic force microscopy (AFM) and grazing incidence x-ray diffraction (GIXRD). We focus on the effects of thermal annealing, acceptor weighting, and alkyl chain length.

Using GIXRD and AFM, we show that PffBT4T-C9C13/fullerene blends have a remarkably unusual fullerene-induced ordering, with an enhanced crystallinity compared to the pristine polymer, contrary to the behaviour displayed by most other conjugated polymers [12, 13]. This crystallinity is further enhanced upon thermal annealing. PffBT4T-2OD/fullerene blends, in contrast, show no fullerene-induced ordering.

PffBT4T-C9C13/fullerene blends display complex transient absorption spectra on microsecond timescales, with clear evidence of polymer triplets that are generated via charge carrier recombination. In addition, two types of polymer polaron are observed: fast-decaying polarons in pristine polymer domains and trapped polarons that decay more slowly and are localised in the crystalline, fullerene-induced ordered domains. All three transient species decay via stretched exponential kinetics: a feature more normally observed in perovskite solar cells [14]. Here, we attribute such kinetics to the spectral proximity of three distinct species, leading to multiple decay pathways. The lifetime of the trapped polarons in PffBT4T-C9C13/fullerene blends is significantly enhanced upon thermal annealing, but the lifetime varies depending upon the balance of ordered/disordered regions. Intriguingly, PffBT4T-2OD/fullerene blends display neither the fullerene-induced ordering nor the correlated trapped polaron, and we relate this to a difference in donor/acceptor miscibility.

2. Experimental

2.1. Materials

PffBT4T-2OD was bought from 1-Material (M_w = 50 000–100 000, PDI = 1.5–2.5), and the PffBT4T-C9C13 was purchased from Ossila (M_w = 123 796, PDI = 1.68). $PC_{60}BM$ (99%) and $PC_{70}BM$ (99%) were bought from Solenne BV. The solvents chlorobenzene (CB, 99.9%), dichlorobenzene (DCB, 99.9%) and the additive 1,8-diiodooctane (DIO) were purchased from Sigma-Aldrich.

2.2. Sample fabrication

The PffBT4T-C9C13:$PC_{70}BM$ (weight ratio 1:1.2) film was prepared from a 10 mg mL^{-1} in CB solution with 3% DIO. The blend PffBT4T-2OD:$PC_{70}BM$ film (weight ratio 1:1.2) was fabricated from a 13 mg mL^{-1} in CB/DCB (1:1 volume ratio) solution with 3% DIO. The pristine PffBT4T-C9C13 and PffBT4T-2OD films were fabricated from 4 mg mL^{-1} and 2 mg mL^{-1} solutions in CB, respectively. The pristine PffBT4T-2OD and PffBT4T- C9C13 solutions were 0.01 mg mL^{-1} in CB. All solutions were initially prepared outside the glovebox and then heated at 100 °C overnight with a stirring rate 500 rpm inside the glovebox. Thin films were made by spin coating inside the glovebox under nitrogen atmosphere. All the glassware used to make thin films was preheated at 100 °C on the hotplate for at least 30 min. The hot solution was then deposited onto 1 cm^2 glass substrates to make thin films at a spin rate of 800 rpm for 60 s. The PffBT4T-C9C13:$PC_{70}BM$ and PffBT4T-2OD:$PC_{70}BM$ blend films were thermal annealed at 80 °C for 5 min on the hotplate. Thermal annealing is a widely used method to improve solar cell efficiency in a wide range of polymers [15–17]. Thermal annealing involves heating the active layer, providing the blend with additional thermal energy. This allows the polymer chains and acceptor molecules to rearrange to acquire a morphology at a

thermodynamic minimum. This therefore promotes lower energy morphologies, which are typically correlated with higher crystallinities.

2.3. Ground state absorption spectroscopy

Ground state absorption spectra of all samples were recorded with a Perkin Elmer Lambda 365 with the range from 300 nm to 1100 nm at ambient atmosphere.

2.4. Photoluminescence (PL) spectroscopy

PL spectra were obtained with Fluorolog-3 Spectrometer (Horiba). The 450 W xenon short arc lamp provided the excitation wavelength of 650 nm. The spectra were measured at 100 accumulated exposures of 0.1 s. Corrections were made by subtracting the background and accounting for the detector and lamp response. PL spectra were normalised per sample absorption at the excitation wavelength.

2.5. TAS

A pump-probe micro-millisecond TA spectroscopy set-up was used to measure the TA spectra and kinetics. Laser pulses (repetition rate 10 Hz, pulse duration 6 ns) were generated by a Nd:YAG laser (Spectra Physics, INDI-40-10). Excitation wavelength was selected by a versaScan L-532 OPO and the excitation density was set in the range between 0.3 and 120 μJ cm^{-2} using neutral density filters, measured by the ES111C power meter (Thorlabs). The probe light was provided by the quartz tungsten halogen lamp (IL1, Bentham). Probe wavelength selectivity was achieved using bandpass filters and a Cornerstone 130 monochromator (Oriel Instrument) before the detector. The TA signals were recorded with Si and InGaAs photodiodes. The signal from the photodiodes was preamplified and sent to the main amplification system with an electronic filter (Costronic Electronics), which was connected to the oscilloscope (Tektronics, DPO4034 B) and PC.

2.6. AFM

AFM images were recorded by Bruker Dimension Icon in ScanAsyst peak force mode. Cantilevers used for AFM were Bruker scanasyst-Air with a nominal radius of 4 nm.

2.7. GIXRD

X-ray diffraction analysis was carried out using a Bruker AXS D8 Advanced x-ray diffractometer in grazing-incidence mode with parallel beam optics equipped with a LynxEye silicon strip detector and copper source (Cu Kα1, 1.54056 Å and Kα2, 1.54439 Å) run at 40 kV, 40 mA. The angular range was 2.5° to 30° 2θ counted at 0.05°/s with data-step of 0.05° using a 1° grazing incident angle (θ) on the films. All the GIXRD samples were spin cast on quartz substrates.

3. Results

3.1. Steady-state absorbance and PL

The polymer structures are shown in figure 1, along with the normalised steady state absorption spectra of pristine PffBT4T-C9C13 and PffBT4T-C9C13:$PC_{70}BM$ films (weight ratio 1:1.2) before and after annealing. The ground state absorption spectra of the pristine PffBT4T-C9C13 solution shows a very strong temperature dependence (figure 1(b)), as seen in previous reports for other PffBT4T polymers [5, 15]. Upon decreasing the temperature from 75 °C to 25 °C, all absorption bands red-shift, and a distinct vibronic structure appears. This indicates the presence of a strong polymer aggregation and enhanced planarity at room temperature.

A qualitative assessment of the PffBT4T-C9C13 film crystallinity can be made from the ratio of the vibronic 695 nm (0-0) and 630 nm (0-1) bands (figure 1(c)). A more rigid structure (which is correlated with greater crystallinity) inhibits structural change during electronic excitation and therefore, according to the Franck–Condon Principle, increases the relative intensity of the (0-0) absorption band. The fullerene blend films appear to exhibit greater crystallinity than the pristine film: an unusual observation. This suggests that the presence of the fullerene is able to impart some order on the system, which is also evidenced by both the red-shift of the 0-0 peak and the sharper absorption onset from the pristine to the blend. Indeed, it has been noted previously that no clear d-spacing is observed in GIWAXS data for analogue pristine PffBT4T-2DT (indicating a tilted π–π stacking structure) [5], while PffBT4T-2DT:$PC_{60}BM$ does show d-spacing, evidence of typical parallel π–π stacking [18]. Our absorbance results suggest that a similar evolution is occurring for PffBT4T-C9C13; this will be explored further in the next section. A similar fullerene-induced ordering has been previously observed for PBTTT:fullerene blends [19], where the intercalation of small fullerenes between the alkyl chains of the polymer produced extensive co-crystallisation. Furthermore, bulkier fullerenes were not able to intercalate, and the resultant PBTTT domains were more amorphous.

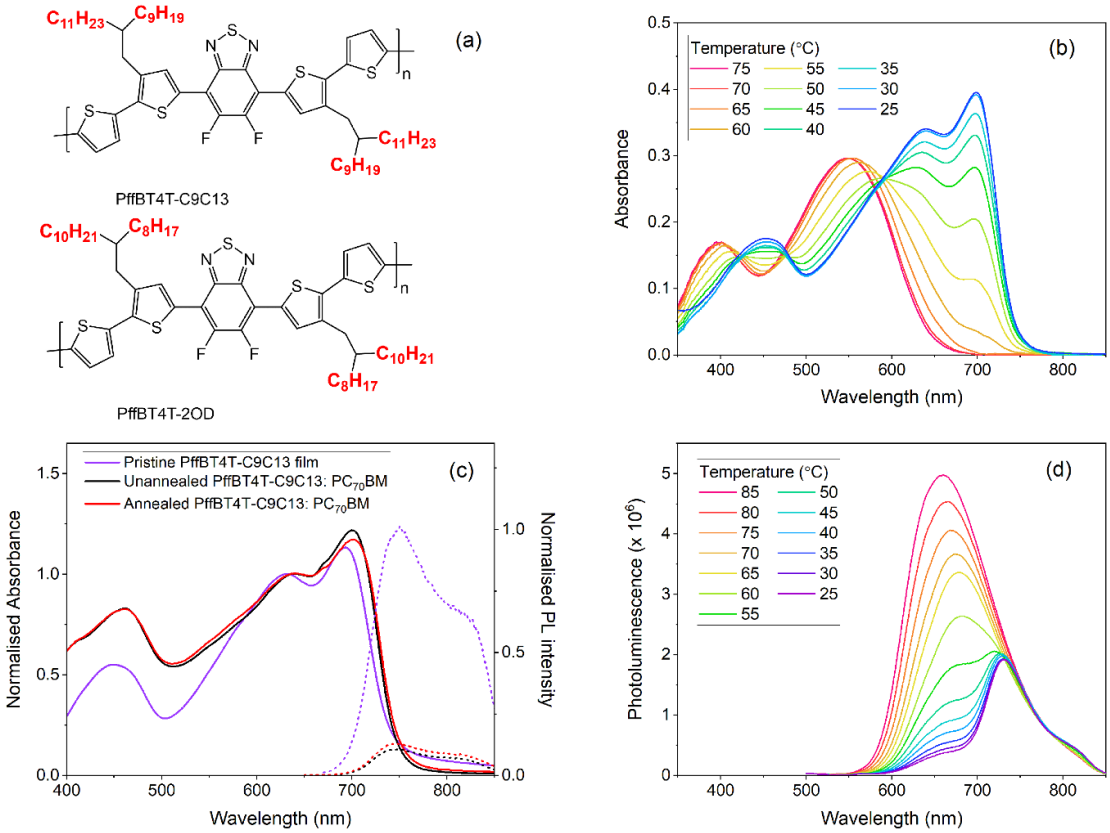

Figure 1. (a) The structures of PffBT4T-C9C13 and PffBT4T-2OD are shown. (b) Temperature-dependent steady state absorption spectra of a pristine PffBT4T-C9C13 solution (0.01 mg mL^{-1} in CB). (c) Normalised steady state absorption spectra (solid lines) for pristine PffBT4T-C9C13 film, unannealed and annealed PffBT4T-C9C13:$PC_{70}BM$ (1:1.2 by weight). Normalised (per absorption) PL emission spectra (dashed lines) for pristine PffBT4T-C9C13, unannealed and annealed PffBT4T-C9C13:PC70BM blend films, with excitation wavelength 650 nm. (d) Temperature-dependent steady state PL spectra of a pristine PffBT4T-C9C13 solution (0.01 mg mL^{-1} in CB).

Figure 1(c) also shows the PL of PffBT4T-C9C13 pristine and $PC_{70}BM$ blend films, with an excitation wavelength of 650 nm. Figure 1(d) shows the temperature dependence of the PffBT4T-C9C13 solution PL. The PL spectral changes mirror those seen in the absorption spectra. Intriguingly, however, the PL displays the presence of two distinct emissive species, rather than a continuous shift. One species emitting at 730 nm corresponds to the fully planar 'aggregated' PffBT4T-C9C13, showing higher intensity at lower temperatures, and the other at 660 nm corresponds to the non-aggregated PffBT4T-C9C13. The 730 nm PL band shows no shifting with temperature, which is consistent with its assignment to a planar, rigid structure. The apparent rise in PL intensity with increasing temperature reflects the relative populations of these two species. Since planar conformers typically have a greater quantum yield of fluorescence, we can assume that the non-aggregated species still has a significant presence even at 25 °C. Conversely, at high temperatures the planar form has largely disappeared. The PL spectrum of the planar, aggregated species in solution (at 25 °C) displays a very strong 0-0 band at 730 nm compared to its 0-1 vibronic band at 800 nm, significantly more so than what was observed in the pristine film (figure 1(c)). The implication is that the pristine PffBT4T-C9C13 film does not possess the same extent of planar structure as the room temperature solution. This loss in ordered structure is consistent with the absorption spectra of the film samples, which show the pristine film to be the least crystalline.

PL spectroscopy can also be used as an indicator of exciton quenching, whereby excitons diffuse to the donor/acceptor interface and undergo electron transfer. The unannealed (as-deposited) PffBT4T-C9C13:$PC_{70}BM$ film PL (figure 1(c)) is quenched by 90%, indicating a high but not complete level of exciton dissociation when the $PC_{70}BM$ is added. A small increase in PL intensity and a consequent decrease in PL quenching to 87% was found in the annealed blend film. These PL quenching results therefore suggest the morphological changes in the sample upon annealing have little impact on the number of excitons that are able to reach the donor:acceptor interface. A possible explanation to this could be that the PffBT4T-C9C13 exciton diffusion length is greater than the domain size, even after annealing, and therefore excitons can easily reach the interface before relaxing to ground state.

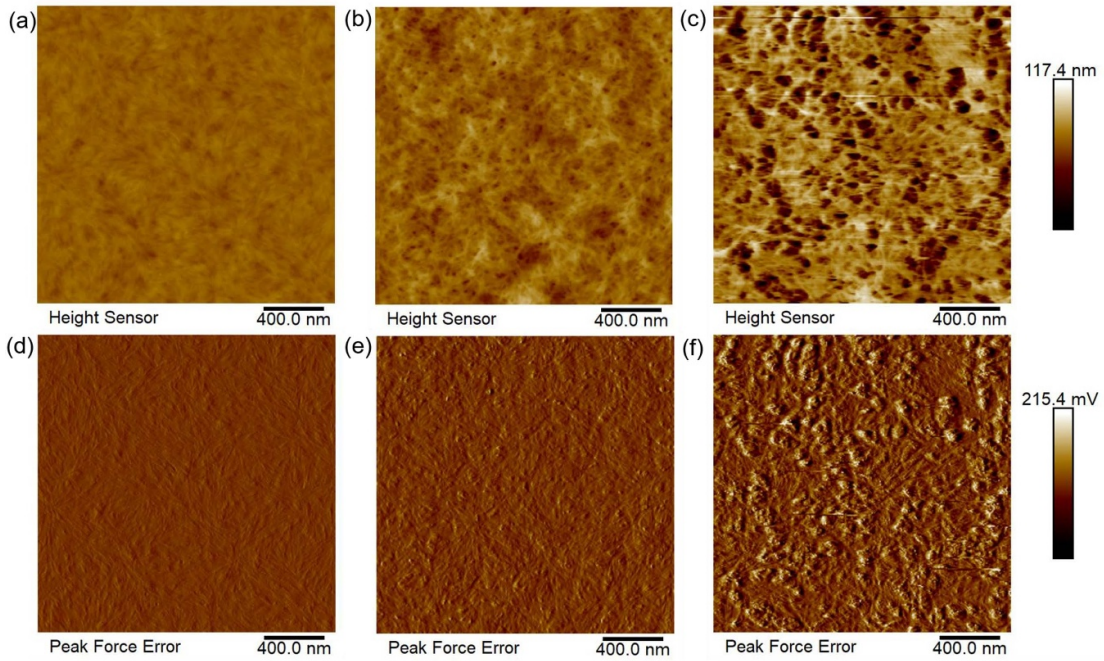

Figure 2. AFM images of phase and topography for (a) and (d) pristine PffBT4T-C9C13, (b) and (e) unannealed PffBT4T-C9C13:$PC_{70}BM$ (1:1.2) and (c) and (f) annealed PffBT4T-C9C13:$PC_{70}BM$ (1:1.2) blend film. Scale bars are 400 nm.

3.2. Morphology

To understand the influence of the addition of $PC_{70}BM$ and thermal annealing to the morphology of PffBT4T-C9C13 films, AFM was used (figure 2). From the height images in figure 2(a)–(c), the average roughness (Ra) increases from the pristine (2.4 nm) to unannealed blend (6.4 nm) to annealed blend film (16 nm). The increased roughness values show that phase segregation is induced by the addition of $PC_{70}BM$ and enhanced via thermal annealing. The topography of these films (figures 2(d)–(f)) clearly shows the formation of larger domains upon thermal annealing.

In addition, GIXRD was performed for PffBT4T-C9C13 and its blend films (figure S1 (available online at stacks.iop.org/JPMATER/4/044009/mmedia)). In general, the signal intensities were substantially reduced compared to literature studies of the analogous PffBT4T-2OD [20], suggesting much less crystalline structures. Indeed, the (010) peak at ~16 cm^{-1} (denoting π–π stacking) for pristine PffBT4T-C9C13 is only weakly apparent. This observation is similar to the predominantly amorphous tilted π–π stacking previously observed for PffBT4T-2DT [5]. In contrast, however, the (010) peak for the PffBT4T-C9C13:$PC_{70}BM$ blend exhibited a significantly greater peak area (by a factor of 1.6 compared to pristine PffBT4T-C9C13, corrected for absorbance). The integrated peak area indicates the relative amount of crystalline polymer domains in the film [20], thereby suggesting a greater crystallinity for the blend compared to the pristine polymer. This is consistent with the steady-state absorbance and AFM results and suggests that this greater crystallinity in the blend is related to fullerene-induced ordering. As such, given that non-unity domain purities have been observed for PffBT4T-C9C13:$PC_{70}BM$ [4], it appears that mixed polymer/acceptor domains for this blend may have a greater crystallinity compared to the polymer-only domains. This is a highly unusual observation: addition of fullerene typically perturbs the crystallinity of a pristine polymer, and mixed domains are usually amorphous. In PffBT4T-C9C13:$PC_{70}BM$, however, the converse is true.

Annealing the PffBT4T-C9C13:$PC_{70}BM$ blend increased the (010) peak area further (by a factor of 1.3 compared to the unannealed blend), suggesting a further enhancement in film crystallinity. This, in addition to the greater domain sizes observed in the AFM, suggest that these fullerene-induced ordered regions become larger. It is curious, therefore, that the steady state absorbance and PL do not show such strong changes with thermal annealing as the morphology techniques. However, it is important to note that the spectroscopy techniques encompass the entire film (~1 cm^2) while the morphology techniques target a small, localised area in greater detail. It has been previously shown by Peng *et al* [21] that strong thermal annealing of PffBT4T-C9C13:$PC_{70}BM$ leads to prominent fullerene extrusion. Although their thermal annealing conditions were more extreme than ours in terms of both temperature and time, a degree of fullerene extrusion cannot be discounted, and this could contribute to the greater phase segregation and

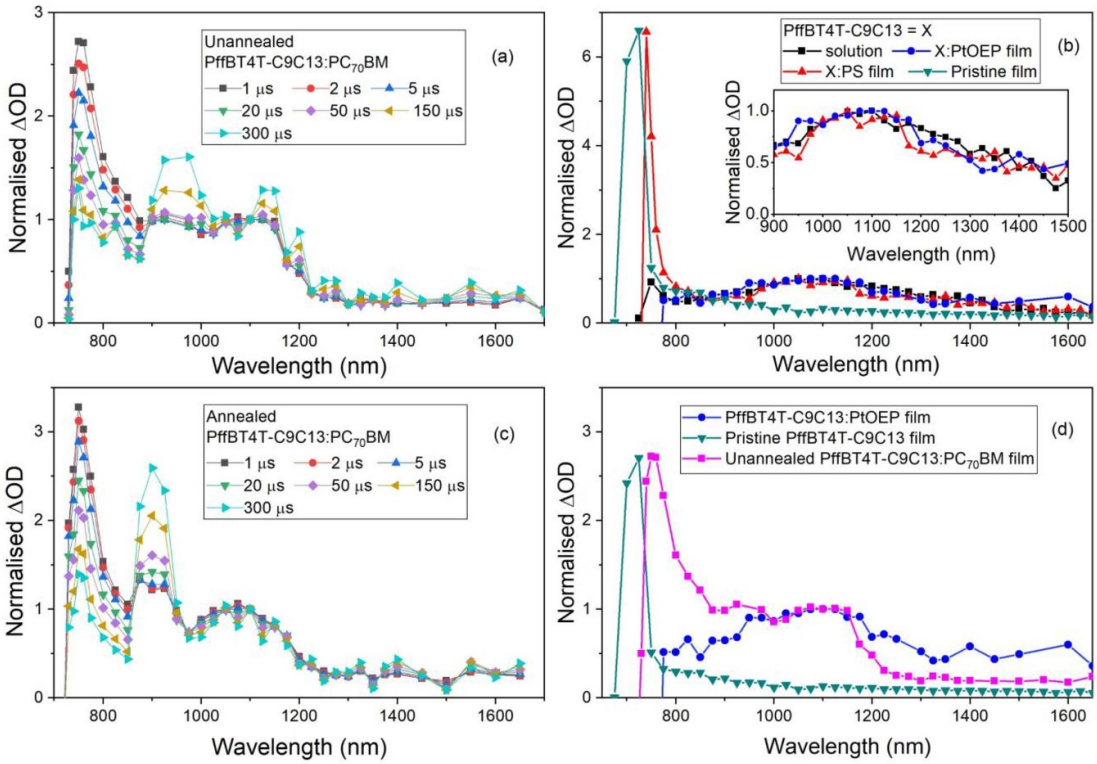

Figure 3. (a) Time evolution of the TA spectra of unannealed PffBT4T-C9C13:PC70BM (1:1.2) blends at different timescales. (b) Normalised transient absorption spectra of pristine PffBT4T-C9C13 solution, film, blend PffBT4T-C9C13:PS (3:2), and PffBT4T-C9C13:PtOEP (3:2) films. (c) Time evolution of the TA spectra of annealed PffBT4T-C9C13:PC70BM blend films at different timescales. (d) Normalised TA spectra of unannealed PffBT4T-C9C13:PC70BM film compared to the control transient spectra. An excitation wavelength of 700 nm and excitation density 4 μJ cm^{-2} was used for both unannealed and annealed PffBT4T-C9C13:PC70BM blend films. An excitation wavelength of 600 nm and excitation densities of 34 μJ cm^{-2} and 114 μJ cm^{-2} were used for both pristine solution and film, respectively. An excitation wavelength of 700 nm and excitation density 65 μJ cm^{-2} were used for the PffBT4T-C9C13:PS (3:2) blend film. An excitation wavelength of 545 nm (to excite the porphyrin) and excitation density 30 μJ cm^{-2} were used for the blend PffBT4T-C9C13:PtOEP (3:2) film.

domain coarsening we observe in the AFM. Since fullerene extrusion and enhanced fullerene-induced ordering—which are not mutually exclusive—have opposing spectroscopic effects (the former decreases the vibronic 0-0/0-1 ratio while the latter increases it), this could account for the lack of change in the steady state absorbance spectra.

3.3. TAS

Microsecond-millisecond TAS was employed to investigate the excited state behaviour of PffBT4T-C9C13 and its blends. Of particular interest are charge generation and recombination processes with respect to thermal annealing. The unannealed and annealed PffBT4T-C9C13:$PC_{70}BM$ blend films are shown in figures 3(a) and (c), normalised to show their spectral evolution over time. Both sets of spectra display three TA bands at <750, 900, and 1100 nm. The bands are more clearly differentiated in the annealed blend, where the 900 nm band becomes increasingly prominent at long times, indicating an enhanced lifetime.

In order to assign these bands, a set of control samples was measured: PffBT4T-C9C13 solution, the pristine polymer film, the polymer dispersed in an inert polystyrene (PS) matrix, and a PffBT4T-C9C13:PtOEP film, where platinum octylethylporpyrin (PtOEP) is a commonly used triplet sensitiser [22]. As displayed in figure 3(b), the TA spectrum of the pristine PffBT4T-C9C13 film shows a single peak at approximately 725 nm, although its proximity to the ground state bleach makes an exact position difficult to establish. This 725 nm band is oxygen insensitive and decays via with power law kinetics (figure S2(a)) and is thus attributed to PffBT4T-C9C13 polarons. The PffBT4T-C9C13 solution exhibits a very different TA spectrum, with a triplet peak at 1080 nm, as evidenced by the strong, reversible oxygen quenching and monoexponential decay kinetics (figure S2(b)). To check for spectral shifting from the solution to the condensed phase, a triplet sensitisation measurement was performed using a PffBT4T-C9C13:PtOEP (3:2) film. By exciting the PtOEP at 545 nm, the lower energy PffBT4T-C9C13 triplet is formed by triplet energy transfer. The TA spectrum of the PffBT4T-C9C13:PtOEP film shows a weak, broad band at 1050 nm. Considering that a PS:PtOEP film with the same ratio exhibits the PtOEP triplet

below 800 nm (figure S2(c)), this 1050 nm band can be confidently assigned to the PffBT4T-C9C13 triplet. Note that both pristine solution and film TA spectra were measured using higher excitation densities than for blend films. This was necessary to achieve acceptable signal/noise ratios. However, altering the excitation density does not create any change in the pristine polymer's TA spectral shape (figure S3) or kinetics (figure S4).

Control PffBT4T-C9C13:PS films were also assessed using a variety of blend ratios. While some ratios (such as 1:1.2) showed only evidence of polarons (*vide infra*), the 3:2 blend showed evidence of polarons and triplets, with both 725 nm and 1050 nm bands appearing (figure 3(b)). The new appearance of the triplet—in contrast to the pristine film, for which solely polarons were observed—could be due to the greater intermolecular interactions in the more condensed films enabling faster triplet-triplet deactivation, leaving a negligible triplet population on μs timescales. Interestingly, the PffBT4T-C9C13 triplet in the PS blend film is substantially less oxygen sensitive compared to the PffBT4T-C9C13 triplet in solution (figure S5). This suggests that the triplet energy level in the condensed phase is lower than in solution (perhaps approaching the oxygen singlet energy), thereby inhibiting the quenching process. Indeed, since the S_1 energy of the pristine PffBT4T-C9C13 film is estimated to be 1.71 eV based on the crossing point of ground state absorption and emission spectra, the T_1 energy can be estimated as ~1.01 eV, which is around the S_1 energy of oxygen (0.98 eV).

Now that the spectral positions of the PffBT4T-C9C13 triplet and polaron have been established, we turn our attention back to the fullerene blends. The <750 nm band matches well with the PffBT4T-C9C13 polaron (figure 3(d)). The PffBT4T-C9C13 triplet spectrum overlaps very well with the 1100 nm band, indicating that the polymer triplet is present in the fullerene blend as well as polarons. However, none of the control samples exhibited the 900 nm band and it is only present in the donor/acceptor blend. The 900 nm band is still present when switching the acceptor from $PC_{70}BM$ to $PC_{60}BM$ (figure S6), indicating that it relates to a PffBT4T-C9C13 species rather than the fullerene (note that the 1100 nm and 750 nm bands also do not shift when altering the acceptor, consistent with their assignments to polymer triplets and polarons respectively, figure 4(a)).

To address the identity of the blend's longer-lived feature at 900 nm, a variety of other experiments were performed, including altering the blend ratio and excitation wavelength. Oxygen sensitivity experiments were inconclusive: as shown previously, the polymer triplet in more condensed phases shows substantially reduced oxygen quenching, and the proximity to the strong oxygen-insensitive polaron band at <750 nm further complicates this. The 900 nm band appears more prominently when the polymer is selectively excited at 700 nm (figure S7), when the fullerene weighting is increased (figure 4(a)), and upon thermal annealing. It is therefore our hypothesis that the 900 nm band is correlated with polymer polarons that are localised in the fullerene-induced ordered domains. This assignment is consistent with the narrowness of the band (the polarons exist in a relatively homogeneous environment) and previous literature assignments of bimodal polarons located in different morphological environments [12].

The presence of three spectrally proximal transient species leads to complex decay kinetics. Figure 4(b) shows the transient absorption decay dynamics of the TA bands at 750, 900 and 1100 nm in PffBT4T-C9C13:$PC_{70}BM$ blend films before and after annealing. For all probe wavelengths, stretched exponential kinetics were observed ($\Delta OD \propto e^{(-t/)^{\beta}}$). Triplets typically exhibit monoexponential kinetics, whilst polarons undergoing diffusion-limited bimolecular recombination exhibit power-law kinetics. In contrast, stretched exponential kinetics are typically associated with multiple decay pathways in a dispersive environment [23, 24]. Note that a stretched exponential with a distribution parameter of $\beta = 1$ is equivalent to a monoexponential decay, while a power law is achieved when β approaches 0. The observation of stretched exponential kinetics for PffBT4T-C9C13:$PC_{70}BM$ blend films is therefore consistent with the observed triplet and polaron overlapping absorption bands, and also the presence of morphological variation. All three transient species display a longer lifetime after annealing. The excitation density dependent kinetics are presented in figure S8.

To assess the relative populations of each transient species, the TA spectra normalised per photon absorbed were assessed for each sample (figure 4(a)). Considering the PffBT4T-C9C13 triplet at 1100 nm, it is immediately apparent that the triplet population is significantly greater in the blends compared to any of the polymer-only samples (3:2 PS blend in figure 4(a); other PS blend ratios, pristine film and solution in figure S9). Indeed, the polymer triplet population also increases when the fullerene loading increases from 10% to 55%. Note that although the $PC_{70}BM$ triplet also absorbs at 1100 nm [25, 26], the strong similarity between the PffBT4T-C9C13:$PC_{60}BM$ and PffBT4T-C9C13:$PC_{70}BM$ spectra indicate that we are observing solely PffBT4T-C9C13 triplets. The enhanced polymer triplet formation in the blend, in comparison with the pristine sample, must therefore arise from charge carrier recombination via a spin-mixing charge-transfer

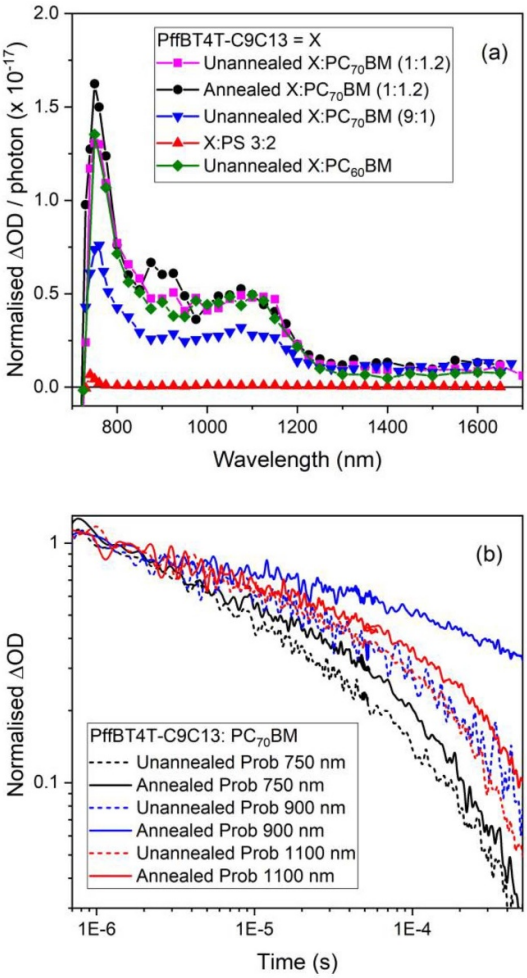

Figure 4. (a) Normalised (per photon absorbed) TA spectra of unannealed PffBT4T-C9C13:$PC_{70}BM$ (1:1.2 and 9:1) and annealed PffBT4T-C9C13: $PC_{70}BM$ (1:1.2), all excited at 700 nm with excitation density around 4 μJ cm^{-2}. An excitation wavelength of 700 nm and excitation density 65 μJ cm^{-2} was used for PffBT4T-C9C13:PS (3:2) blend film. An excitation wavelength of 700 nm and excitation density 11 μJ cm^{-2} was used for PffBT4T-C9C13:$PC_{60}BM$ (1:1.2) blend film. All spectra were obtained at 1 μs. (b) Normalised (to 1 at 1 μs) decay dynamics of unannealed and annealed PffBT4T-C9C13:$PC_{70}BM$ (1:1.2) blend films at probe wavelengths of 750 nm, 900 nm, and 1100 nm, with an excitation wavelength of 700 nm and excitation density 4 μJ cm^{-2}.

state. The higher polaron population in blend systems leads to an enhancement of triplet population through this back-transfer process, as has been observed in other OPV blends [22, 27–29]. The triplet population is unaffected by annealing (figure 4(a)) or acceptor identity.

Thermal annealing of the PffBT4T-C9C13:$PC_{70}BM$ 1:1.2 blend increases the two polaron populations at 1 μs, consistent with the longer charge carrier lifetimes observed. The fullerene-induced ordering polaron at 900 nm has a greater relative population increase (∼40%) compared to the 750 nm polaron (∼20%) upon annealing. This is consistent with the morphology data, in which we concluded that the enhanced crystallinity and domain size upon annealing is related to a greater predominance of the fullerene-induced ordered regions. As such, thermal annealing of PffBT4T-C9C13 does enhance charge carrier populations on the timescales relevant to charge extraction in a device, but the significant increase in phase segregation observed in the AFM mean that the trapped polarons may be unable to be extracted efficiently.

3.4. Comparison to PffBT4T-2OD

Now that the photophysics of PffBT4T-C9C13 and its blends have been established, we compare its behaviour to PffBT4T-2OD, which differs from the former with side chain length only. The ground state absorption spectra of pristine PffBT4T-2OD and its unannealed $PC_{70}BM$ blend are very similar and do not exhibit the small red-shift and absorption onset sharpening observed for PffBT4T-C9C13 (figure 5(a)). This suggests that the fullerene-induced ordering is no longer present for PffBT4T-2OD, which is consistent with its greater ordering and crystallinity in the pristine polymer [30].

The TA spectrum of unannealed PffBT4T-2OD:$PC_{70}BM$ (figure 5(c)) is identical to PffBT4T-C9C13: $PC_{70}BM$ in terms of spectral position and shape of the <750 nm and 1100 nm bands, consistent with the very

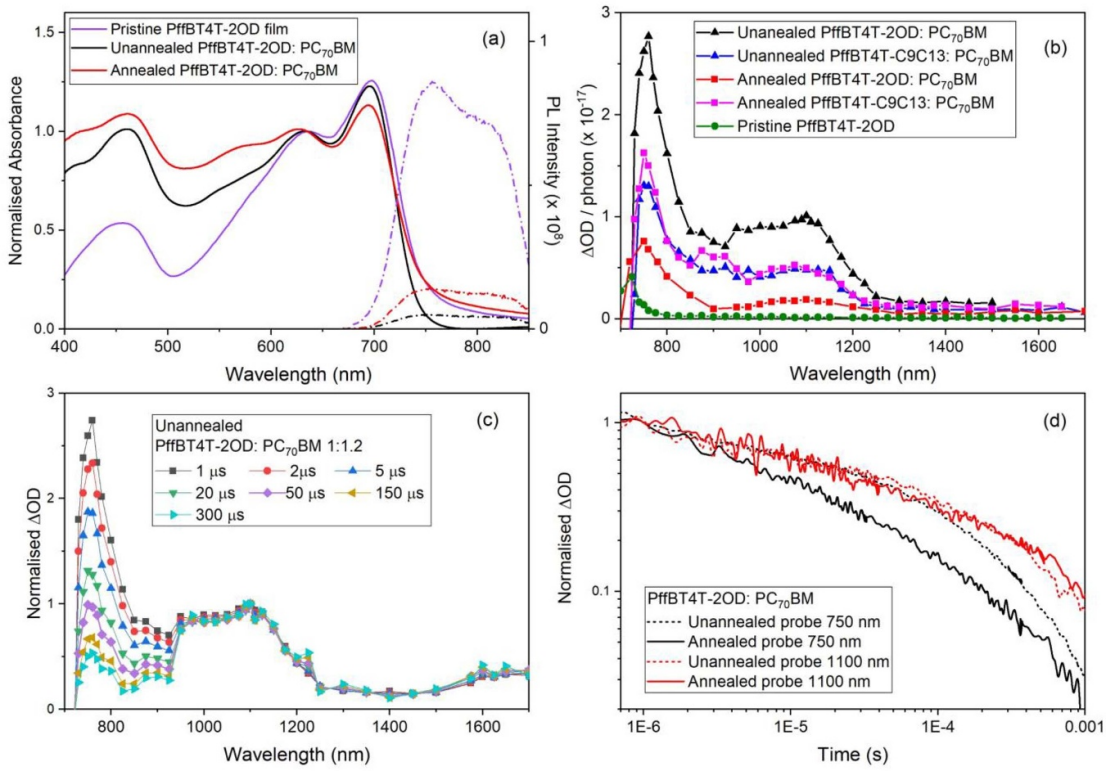

Figure 5. (a) Normalised (to 1 at 635 nm) steady state absorption for pristine PffBT4T-2OD film, unannealed and annealed PffBT4T-2OD:$PC_{70}BM$ (w/t 1:1.2) (solid lines). Normalised (per absorption) PL emission spectra for pristine PffBT4T-2OD, unannealed and annealed PffBT4T-2OD: $PC_{70}BM$ blend films, obtained with excitation at 650 nm (dashed lines). (b) Normalised (per photon absorbed) TA spectra comparison of pristine PffBT4T-2OD film and unannealed and annealed PffBT4T-2OD:$PC_{70}BM$ and PffBT4T-C9C13:$PC_{70}BM$ blends (1:1.2) with excitation wavelength 700 nm at 1 μs. (c) Spectral evolution of unannealed PffBT4T-2OD:$PC_{70}BM$ blend film excited at 700 nm with excitation density around 4 μJ cm^{-2}. (d) Normalised (to 1 at 1 μs) decay dynamics of unannealed and annealed PffBT4T-2OD: $PC_{70}BM$ blend, obtained with probe wavelengths of 750 nm and 1100 nm with excitation wavelength 700 nm and excitation density 4 μJ cm^{-2}.

small structural change in the polymer which is unlikely to affect electronic structure. As such, we can once again assign the <750 nm band to polarons and the 1100 nm band to triplets. Note that in previous spectroscopy reports of PffBT4T-2OD:$PC_{70}BM$ using ps-TAS, the 1100 nm band was assigned to polarons [8, 31]. Our assignment of this band to triplets shows the importance of using longer time TAS to definitively assign peaks and—importantly—assess the contributions of triplets, which is more difficult to accomplish on ultrafast timescales. Our results show, for example, that thermal annealing has little effect on the triplet decay kinetics for PffBT4T-2OD:$PC_{70}BM$ (figure 5(d)). As such, while the triplet population scales proportionally with the polaron population (consistent with the polaron back recombination formation mechanism), the triplets decay independently of the surrounding crystallinity of their environment. This behaviour is in accordance with a monomolecular process such as triplet relaxation where crystallinity plays a minor role, in contrast to bimolecular processes like polaron recombination.

Although the <750 nm and 1100 nm bands in the TA spectra are identical when comparing unannealed PffBT4T-2OD:$PC_{70}BM$ and PffBT4T-C9C13:$PC_{70}BM$, there are a number of differences between the two systems in terms of transient populations and kinetics, particularly upon thermal annealing. While PffBT4T-2OD:$PC_{70}BM$ shows a substantially higher polaron population at 750 nm (1 μs) compared to PffBT4T-C9C13:$PC_{70}BM$, thermal annealing decreases the polaron population by a factor of 3.5 (figure 5(b)). For PffBT4T-C9C13:$PC_{70}BM$, in contrast, thermal annealing does not strongly influence the 750 nm polaron population. The similar polaron/triplet ratio between the two blend systems suggests that polaron back recombination occurs to a similar extent in both systems and thus this cannot be the reason for the difference in behaviour. AFM of PffBT4T-2OD:$PC_{70}BM$ blends shows that the average surface roughness scarcely changes upon thermal annealing (5.6 nm to 5.2 nm) as displayed in figure S10. However, Zhang *et al* have previously pointed out that the surface morphology of PffBT4T-2OD:$PC_{70}BM$ is not representative of the bulk morphology for this blend, and that correlation lengths do indeed increase upon annealing [6]. An examination of PL quenching yields for PffBT4T-2OD:$PC_{70}BM$ show a reduction in quenching from 94% to 84% upon thermal annealing (figure 5(a)); the concomitant decrease in exciton quenching could partially account for the smaller polaron yield. Furthermore, a consideration of the decay kinetics (figure 5(d)) shows

that the PffBT4T-2OD polaron decays considerably faster after annealing (the reverse is true for PffBT4T-C9C13). Given the similar polaron/triplet ratio, this suggests that upon annealing the PffBT4T-2OD polymer polaron has an additional decay pathway: likely fast geminate recombination back to the ground state in the more crystalline, polymer-rich regions of the film (noting that charge generation is present in the pristine PffBT4T-2OD film itself).

It is notable that there is no evidence of the 900 nm band for PffBT4T-2OD:$PC_{70}BM$, neither before nor after annealing. This is consistent with this band's assignment to polymer polarons localised in fullerene-induced ordered regions in the PffBT4T-C9C13:$PC_{70}BM$ blend: no such fullerene-induced ordering was observed for PffBT4T-2OD.

4. Discussion

Unusually, PffBT4T-C9C13:$PC_{70}BM$ blends display enhanced crystallinity compared to the pristine polymer and this induces some intriguing spectroscopic behaviour. The sharp 900 nm TA band observed for PffBT4T-C9C13:$PC_{70}BM$ has been assigned to polarons localised in the crystalline, fullerene-induced ordered domains. This assignment is consistent with the increased intensity of the 900 nm band with fullerene weighting and the changes in the ground state absorbance spectra. Importantly, this assignment is also consistent with the absence of the fullerene-induced ordering for PffBT4T-2OD:$PC_{70}BM$ and subsequent absence of the 900 nm band.

Thermal annealing induces greater phase segregation and enhanced crystallinity of the PffBT4T-C9C13:$PC_{70}BM$ blend. This correlates with an enhanced lifetime of the 900 nm (ordered) polymer polaron. However, while the 900 nm band appeared reproducibly across all annealed blend samples trialled, it was noted that it was increasingly longer-lived with reduced vibronic 0-0/0-1 peak ratios (across the natural sample-to-sample variation, figure S11). While this reduced vibronic ratio could indicate lower crystallinity, as explained for figure 1(c), Peng *et al*'s work suggest that this could also be due to increases in fullerene extrusion [21], which can occur upon thermal annealing. The decrease in the 900 nm band's stretched exponential distribution parameter β upon annealing ($\beta = 0.34$ to $\beta = 0.25$) suggests an increased contribution from a power law decay. Since the presence of a power law is related to a Gaussian tail of trap states, these results imply that the ordered polarons in the annealed blend are more influenced by trap states; this would explain the sensitivity of this polaron's lifetime to the local morphology. This could have profound OPV device implications in terms of efficient extraction of charge carriers.

An intriguing point is why PffBT4T-C9C13:$PC_{70}BM$ displays this fullerene-induced ordering and consequent trapped polaron in the blend, whilst PffBT4T-2OD:$PC_{70}BM$ does not. PffBT4T-2OD has a marginally shorter alkyl chain length, and it has been shown that this can lead to changes in film morphology. Face-on orientations become more pronounced compared to edge-on with longer alkyl chain lengths [4, 32] and, furthermore, donor/acceptor miscibility reduces [33]. While orientation relative to the substrate is critical for organic solar cell performance, it is less relevant for optical spectroscopy (when polarisation effects are excluded, as is the case here) and thus cannot account for the observed spectroscopic differences between PffBT4T-C9C13 and PffBT4T-2OD. Miscibility of the fullerene, however, could have a large impact because donor/acceptor spatial separations affect both charge photogeneration and recombination processes. A greater miscibility for PffBT4T-2OD:$PC_{70}BM$ is consistent, for example, with the observation of a larger polaron yield at 1 μs for unannealed PffBT4T-2OD:$PC_{70}BM$ compared to PffBT4T-C9C13:$PC_{70}BM$, and the greater PL quenching. It is therefore possible that the absence of the fullerene-induced polymer polaron in PffBT4T-2OD:$PC_{70}BM$ is related to this greater miscibility.

Another important aspect, observed for both PffBT4T-C9C13:$PC_{70}BM$ and PffBT4T-2OD:$PC_{70}BM$, is the pronounced polymer triplet formation. Because the polymer triplet population scales proportionally with polaron population, and also increases with fullerene weighting, it is most likely that the triplets are being formed from charge carrier recombination, as discussed previously [29]. Whether this is dominated by geminate or non-geminate triplet formation is unknown. However, considering that the 1100 nm triplet band is also observed in ultrafast spectroscopy, having been assigned to polarons in previous literature reports for other PffBT4T polymers [8, 31, 34], this suggests that fast geminate recombination is likely to play a role for these blends. However, a contribution from non-geminate recombination is also highly likely. A comparison of the triplet decay kinetics on μs timescales (figure S12) shows that the fullerene blends' polymer triplets decay much more slowly compared to the inert polystyrene blend's polymer triplet (which must only be formed via standard intersystem crossing). The implication of this is that the polymer triplet population in the fullerene blends is being regenerated via non-geminate charge recombination simultaneously with its decay, thereby retarding the overall kinetics. However, it is noteworthy that non-geminate triplet formation may not affect device performance if charge carrier mobilities are high enough: charges can be extracted prior to the recombination process [35].

The identification of significant triplet populations in PffBT4T-C9C13:$PC_{70}BM$ and PffBT4T-2OD:$PC_{70}BM$ blends, both of which are capable of >10% device efficiencies, is therefore an important step. Not only does it highlight the value of TAS on microsecond timescales, but it also reveals yet more high efficiency blends in which triplets are present to a significant level, across all timescales [36]. In the case of PffBT4T-C9C13:$PC_{70}BM$ and PffBT4T-2OD:$PC_{70}BM$ blends, the triplet kinetics change very little or not at all upon thermal annealing, suggesting that despite being formed via charge carrier recombination (presumably at a donor/acceptor interface), they become primarily localised within pristine polymer domains that are unaffected by annealing (annealing of pristine PffBT4T polymer films is known to induce negligible morphological changes [34]). The polymer triplet decay kinetics are also similar with lower fullerene weightings (figure S12), and in $PC_{60}BM$ blends, which is also consistent with this conclusion. This sequestration into the pristine polymer domains is likely to mean that the energy is lost, and thus the charge recombination in this case is a loss pathway.

Finally, we relate the comparison of PffBT4T-C9C13:$PC_{70}BM$ and PffBT4T-2OD:$PC_{70}BM$ blends to their device performance. Despite the large differences in photophysics observed here, the two blends have very similar device efficiencies, with annealed PffBT4T-2OD:$PC_{70}BM$ showing slightly higher efficiency (10.0%) compared to PffBT4T-C9C13:$PC_{70}BM$ (9.3%) [4]. Assuming the two polymer polarons have similar absorption cross-sections, annealed PffBT4T-C9C13:$PC_{70}BM$ displays a greater polaron population at 750 nm at 1 μs and slower decay kinetics compared to PffBT4T-2OD:$PC_{70}BM$. However, we have shown that PffBT4T-C9C13:$PC_{70}BM$ is substantially less crystalline than PffBT4T-2OD:$PC_{70}BM$, and this is likely to be accompanied by a reduced charge carrier mobility [4, 37, 38]. Since the mobility-lifetime product ($\mu\tau$) is often considered a figure of merit in determining device performance [39], these two factors may cancel one another out, essentially leading to the similar device performances. It should also be noted that PffBT4T-2OD:$PC_{70}BM$ displays an unusual field-assisted exciton separation and thus would exhibit greater charge generation in an operational device [40].

5. Conclusions

In this paper we present a morphology and spectroscopic study of PffBT4T-C9C13 and its fullerene blends before and after annealing. Unusually, the pristine polymer film displays the lowest crystallinity, with the significant enhancement in crystallinity in the blend attributed to fullerene induced ordering and a greater predominance of π–π stacking. Thermal annealing of the blend led to even greater enhancements in film crystallinity and phase segregation.

On microsecond timescales, evidence of polymer triplets generated via charge carrier recombination is observed for PffBT4T-C9C13:$PC_{70}BM$, both before and after thermal annealing. Bimodal polymer polarons are also observed: fast-decaying polarons in pristine polymer domains and polarons localised in the fullerene-induced ordered regions, which decay more slowly. The lifetime of the latter polaron is strongly morphology-dependent and displays characteristics of trapping. All three transient species decayed via stretched exponential kinetics, not at all common for OPV materials. Here, we attribute such kinetics to the spectral proximity of three distinct species in different morphologies, leading to multiple decay pathways.

PffBT4T-2OD—which varies from PffBT4T-C9C13 by only the alkyl chain length—displays quite different spectral behaviour. No evidence of fullerene-induced ordering is observed, and this is accompanied by the loss of the trapped polymer polaron at 900 nm: these observations were attributed to enhanced donor/acceptor miscibility for PffBT4T-2OD. Despite the large differences in photophysics, a comparison to literature shows that PffBT4T-C9C13 and PffBT4T-2OD based solar cells exhibit similar device performances. We attribute this to the more amorphous PffBT4T-C9C13 blend possessing both slower charge carrier recombination kinetics but also lower charge carrier mobility. This highlights how crystallinity and polymer miscibility leads to large changes in charge generation, recombination, and mobility for two very similar materials in terms of chemical structure, demonstrating how morphology control is key for OPV device efficiency.

Data availability statement

All data that support the findings of this study are included within the article (and any supplementary files).

Acknowledgments

TMC would like to acknowledge support from EPSRC project EP/N026411/1.

ORCID iDs

Junjun Guo https://orcid.org/0000-0002-4458-2597
Jose M Marin-Beloqui https://orcid.org/0000-0003-1762-5595
Tracey M Clarke https://orcid.org/0000-0003-4943-0645

References

[1] Darling S B and You F 2013 *RSC Adv.* **3** 17633–48
[2] Liu Q *et al* 2020 *Sci. Bull.* **65** 272–5
[3] Tang C W 1986 *Appl. Phys. Lett.* **48** 183–5
[4] Zhao J, Li Y, Yang G, Jiang K, Lin H, Ade H, Ma W and Yan H 2016 *Nat. Energy* **1** 15027
[5] Chen Z, Cai P, Chen J, Liu X, Zhang L, Lan L, Peng J, Ma Y and Cao Y 2014 *Adv. Mater. Weinheim* **26** 2586–91
[6] Zhang Y, Parnell A J, Pontecchiani F, Copper J F K, Thompson R L, Jones R A L, King S, Lidzey D and Barnado G 2017 *Sci. Rep.* **7** 44269
[7] Zhang Y, Parnell A J, Blaszczyk O, Musser A J, Samuel I D W, Lidzey D G and Bernardo G 2018 *Phys. Chem. Chem. Phys.* **20** 19023–9
[8] Cha H, Wheeler S, Holliday S, Dimitrov S D, Wadsworth A, Lee H H, Baran D, McCulloch I and Durrant J R 2018 *Adv. Funct. Mater.* **28** 1–11
[9] Clarke T M, Ballantyne A, Shoaee S, Soon Y W, Duffy W, Heeney M, McCulloch I, Nelson J and Durrant J R 2010 *Adv. Mater. Weinheim* **22** 5287–91
[10] Cha H, Tan C-H, Wu J, Dong Y, Zhang W, Chen H, Rajaram S, Narayan K S, McCulloch I and Durrant J R 2018 *Adv. Energy Mater.* **8** 1801537
[11] Marin-Beloqui J M, Fallon K J, Bronstein H and Clarke T M 2019 *J. Phys. Chem. Lett.* **10** 3813–9
[12] Guo J, Ohkita H, Yokoya S, Benten H and Ito S 2010 *J. Am. Chem. Soc.* **132** 9631–7
[13] Ohkita H *et al* 2008 *J. Am. Chem. Soc.* **130** 3030–42
[14] DeQuilettes D W, Vorpahl S M, Stranks S D, Nagaoka H, Eperon G E, Ziffer M E, Snaith H J and Ginger D S 2015 *Science* **348** 683–6
[15] Hu H, Chow P C Y, Zhang G, Ma T, Liu J, Yang G and Yan H 2017 *Acc. Chem. Res* **50** 2519–28
[16] Rait S, Kashyap S, Bhatnagar P K, Mathur P C, Sengupta S K and Kumar J 2007 *Sol. Energy Mater. Sol. Cells* **91** 757–63
[17] Karuthedath S *et al* 2018 *J. Mater. Chem.* A **6** 7428–38
[18] Baran D *et al* 2016 *Energy Environ. Sci.* **9** 3783–93
[19] Mayer A C, Toney M F, Scully S R, Rivnay J, Brabec C J, Scharber M, Koppe M, Heeney M, McCulloch I and McGehee M D 2009 *Adv. Funct. Mater.* **19** 1173–9
[20] Liu Y, Zhao J, Li Z, Mu C, Ma W, Hu H, Jiang K, Lin H, Ade H and Yan H 2014 *Nat. Commun.* **5** 5293
[21] Peng Z, Jiao X, Ye L, Li S, Rech J J, You W, Hou J and Ade H 2018 *Chem. Mater.* **30** 3943–51
[22] Etzold F, Howard I A, Forler N, Melnyk A, Andrienko D, Hansen M R and Laquai F 2015 *Energy Environ. Sci.* **8** 1511–22
[23] Albero J, Zhou Y, Eck M, Rauscher F, Niyamakom P, Dumsch I, Allard S, Scherf U, Krüger M and Palomares E 2011 *Chem. Sci.* **2** 2396–401
[24] Nelson J 1999 *Phys. Rev. B* **59** 15374–80
[25] Keiderling C 2017 PhD Thesis Imperial College London
[26] Chow P C Y, Albert-Seifried S, Gélinas S and Friend R H 2014 *Adv. Mater. Weinheim* **26** 4851–4
[27] Chen M, Krzyaniak M D, Nelson J N, Bae Y J, Harvey S M, Schaller R D, Young R M and Wasielewski M R 2019 *Proc. Natl Acad. Sci. USA* **116** 8178–83
[28] Gillett A J *et al* 2020 (arXiv:2010.10978)
[29] Dimitrov S D *et al* 2015 *Nat. Commun.* **6** 1–8
[30] Ma W *et al* 2015 *Adv. Energy Mater.* **5** 1501400
[31] Dong Y, Cha H, Zhang J, Pastor E, Tuladhar P S, McCulloch I, Durrant J R and Bakulin A A 2019 *J. Chem. Phys.* **150** 104704
[32] Li M, Leenaers P J, Wienk M M and Janssen R A J 2020 *J. Mater. Chem.* C **8** 5856–67
[33] Ma R *et al* 2020 *Sol.* RRL **4** 2000250
[34] Zhang W, Hu R, Zeng X, Su X, Chen Z, Zou X, Peng J, Zhang C and Yartsev A 2019 *Polymers* **11** 408
[35] Schlenker C W *et al* 2012 *J. Am. Chem. Soc.* **134** 19661–8
[36] Karuthedath S, Gorenflot J, Melianas A, Kan Z, Kemerink M and Laquai F 2020 *J. Phys. Chem. Lett.* **11** 2838–45
[37] Woo C H, Piliego C, Holcombe T W, Toney M F and Fréchet J M J 2012 *Macromolecules* **45** 3057–62
[38] McGehee M D, Cates N C, Gysel R, Dahl J E P and Sellinger A 2010 *Chem. Mater.* **22** 3543–8
[39] Vijila C *et al* 2013 *J. Appl. Phys.* **114** 184503
[40] Weu A, Hopper T R, Lami V, Kreß J A, Bakulin A A and Vaynzof Y 2018 *Chem. Mater.* **30** 2660–7